Loop-closure kinetics reveal a stable, right-handed DNA intermediate in Cre recombination

Massa J. Shoura[1,2], Stefan M. Giovan[2], Alexandre A. Vetcher[2], Riccardo Ziraldo[1], Andreas Hanke[3] and Stephen D. Levene [1,2,4,*]

[1]Department of Bioengineering, University of Texas at Dallas, Richardson, TX 75080, USA, [2]Department of Biological Sciences, University of Texas at Dallas, Richardson, TX 75080, USA, [3]Department of Physics, University of Texas Rio Grande Valley, Brownsville, TX 78520, USA and [4]Physics, University of Texas at Dallas, Richardson, TX 75080, USA

ABSTRACT

In Cre site-specific recombination, the synaptic intermediate is a recombinase homotetramer containing a pair of loxP DNA target sites. The enzyme system's strand-exchange mechanism proceeds via a Holliday-junction (HJ) intermediate; however, the geometry of DNA segments in the synapse has remained highly controversial. In particular, all crystallographic structures are consistent with an achiral, planar Holliday-junction (HJ) structure, whereas topological assays based on Cre-mediated knotting of plasmid DNAs are consistent with a right-handed chiral junction. We use the kinetics of loop closure involving closely spaced (131–151 bp) loxP sites to investigate the *in-aqueo* ensemble of conformations for the longest-lived looped DNA intermediate. Fitting the experimental site-spacing dependence of the loop-closure probability, *J,* to a statistical-mechanical theory of DNA looping provides evidence for substantial out-of-plane HJ distortion, which unequivocally stands in contrast to the square-planar intermediate geometry from Cre-loxP crystal structures and those of other int-superfamily recombinases. *J* measurements for an HJ-isomerization-deficient Cre mutant suggest that the apparent geometry of the wild-type complex is consistent with temporal averaging of right-handed and achiral structures. Our approach connects the static pictures provided by crystal structures and the natural dynamics of macromolecules in solution, thus advancing a more comprehensive dynamic analysis of large nucleoprotein structures and their mechanisms.

INTRODUCTION

Changes in DNA topology, manifested by properties such as supercoiling, knotting and catenation, are integral to numerous cellular processes including DNA replication, transcription and recombination (1–7). Using circular DNA as a model system to investigate these processes allows associated topological changes to be readily characterized by established biophysical techniques such as gel electrophoresis (8–10). However, drawing a connection between changes in topological parameters and perturbations of canonical DNA geometry is not straightforward for several reasons. First, geometric solutions consistent with a given topology are rarely unique. This is the case with DNA supercoiling, for example, for which the sum of DNA twist and writhe (i.e. the linking number) is conserved, but not the individual values of those parameters. Partly because of this ambiguity, relating enzyme-mediated changes in DNA topology to DNA geometry often requires assumptions about the geometries of nucleoprotein intermediates in the enzymatic pathway (11,12). Such assumptions can be difficult to confirm independently through measurements in solution; moreover, atomic-resolution crystallographic structures are not always helpful in resolving structural ambiguities because of inherently limited information about conformational dynamics. Thus, nuances such as conformational changes in the context of a cellular environment may not be fully revealed. Finally, in order to engineer molecular conformations having specific functions, for example, constructing DNA circles having specified geometry and/or topology, there is value in knowing the precise configuration (position in space, orientation and chirality) of DNA segments bound to the enzyme along with information about the conformational dynamics of the nucleoprotein structure (13–15).

The Cre-recombination system of bacteriophage P1 has become an important tool for the genetic manipulation of higher organisms (16) and is a paradigm for site-specific DNA-recombination mechanisms employed by the λ-integrase (λ-int) superfamily of recombinases (17,18). In the life cycle of phage P1 Cre plays a critical role in genome maintenance by unlinking newly replicated sister chromosomes to ensure their proper segregation following DNA replication (19). Cre acts at a 34-bp wild-type DNA recombination-target sequence called loxP, which consists of 13-bp perfect inverted repeats flanking a non-palindromic 8-bp core region (20). The core sequence defines the loxP site's absolute orientation. On a linear DNA molecule Cre-mediated recombination involving a pair of tandemly repeated loxP sequences generates a pair of deletion products (one linear, one circular), each bearing a single copy of loxP (Figure 1). DNA-cleavage steps involve a phosphotyrosine intermediate similar to those employed by type-IB topoisomerases (21). As with other members of the λ-int superfamily, recombination takes place via two successive rounds of DNA-strand cleavage and exchange steps that respectively generate and resolve a four-stranded, Holliday-junction (HJ) DNA intermediate (20,22).

High-resolution crystal structures of Cre synaptic complexes formed with duplex and junction DNAs provided the first insights into mechanistic details of recombination in these systems. On the basis of these structures, the chemical steps in Cre recombination have been explained in terms of DNA strand exchanges taking place within a 2-fold-symmetric, nearly square-planar arrangement of the DNA duplexes (18,22–28). There is, however, a major still-unresolved disagreement between the square-planar exchange mechanism and evidence for a chiral recombination intermediate from topological studies of the Cre reaction on circular DNAs. Analyses of the chirality biases in knotted Cre-recombination products (and also those generated by the mechanistically similar yeast recombinase Flp) strongly suggest that the synaptic intermediate involves a right-handed crossing of target sites (29). A chirality bias is also supported by atomic-force microscopy (AFM) images of synaptic complexes formed on circular DNAs (30) although the handedness of crossings in the complex could not be determined in those experiments. Studies employing tethered single-molecule techniques have sought to address the dynamics of the Cre-loxP synapse in solution (31–34), but are potentially subject to various artifacts that arise from the tethering constraint (35). Thus, information about the structure of the Cre synaptic complex free in solution, as opposed to the crystal form or another immobilized state, has not been available.

To address this disagreement, we investigated the *in-aqueo* (in-solution) ensemble of conformations for the longest-lived looped DNA intermediate in Cre recombination. Time-dependent FRET measurements of donor-fluorophore quenching (36) gave kinetic data for the initial steps of intramolecular Cre-loxP recombination reactions. These measurements were made for each member of a set of twenty linear-DNA constructs each bearing a pair of closely spaced (center-to-center distances 131–151 bp), directly repeated loxP sites. As in our previous work, we analyzed the FRET data using a multi-step kinetic model, which was solved numerically to obtain association and dissociation rate constants for the Cre-loxP synapse. The loop-closure probability, J, a thermodynamic quantity, obtains as a quotient of the rate constants extracted from this kinetic analysis; moreover, the dependence of J on loop size for this homologous series of small semiflexible looped intermediates provides precise structural information about the longest-lived intermediate involved in recombination-site synapsis. By fitting a statistical–mechanical theory for loop closure to the experimental J values (37–39), we obtained a well-defined set of geometric parameters that describe the conformational ensemble of Cre-loxP synapse structures encompassing the minimum mechanical-energy conformation of the longest-lived intermediate complex.

The energy-minimized structure places the loxP half sites in the recombinase–DNA complex at the base of a looped DNA conformation that has close to the 90° internal angle observed in Cre-loxP co-crystal structures (22,26,28). However, the average dihedral angle relating bent DNA segments at the loop ends amounts to a right-handed crossing of ∼66°, suggesting a substantial departure from planar-intermediate geometry. We obtained a similar geometry for synaptic complexes formed by a mutant Cre protein that is defective in HJ resolution, strongly suggesting that formation of the right-handed synapse occurs during early phases of site pairing and strand exchange.

Our experiments in solution thereby provide a structural model consistent with the right-handed chirality of Int-superfamily recombination sites inferred from the combination of topological methods and tangle solutions from knot theory (29). Applied to Cre recombinase and other biological systems such as DNA-binding proteins interacting with chromatin, this approach bridges the static pictures provided by crystal structures and the natural conformational flexibility of macromolecules both *in vitro* and in *vivo*.

MATERIALS AND METHODS

Plasmid DNAs

A series of plasmids pCS2DloxP(n) were constructed by inserting DNA fragments with lengths ($n - 34$) bp, which were derived by PCR amplification from the bacteriophage lambda genome, between the PstI and NotI sites of pCS2DloxP (40). For example, plasmid pCS2DloxP(130) was constructed by inserting a 96-bp DNA fragment between the two loxP sites as described. Cloning steps were confirmed by didexoynucleotide sequencing. Plasmids were propagated in *Escherichia coli* HB101 cells and isolated in quantity by using a Promega Wizard Plus Megaprep purification kit (Promega Corp., Madison, WI).

Fluorescently labeled DNAs

Donor and acceptor fluorophores were incorporated into DNA fragments using PCR. Plasmids from the pCS2DloxP(n) family were linearized by ScaI treatment and used as templates. Atto 647N- and Atto 594-labeled oligonucleotides were used as forward and reverse primers, respectively. The primers were purchased from IBA (Göttingen, Germany) and were purified twice by reverse-phase HPLC. PCR reactions were carried out using *Taq*
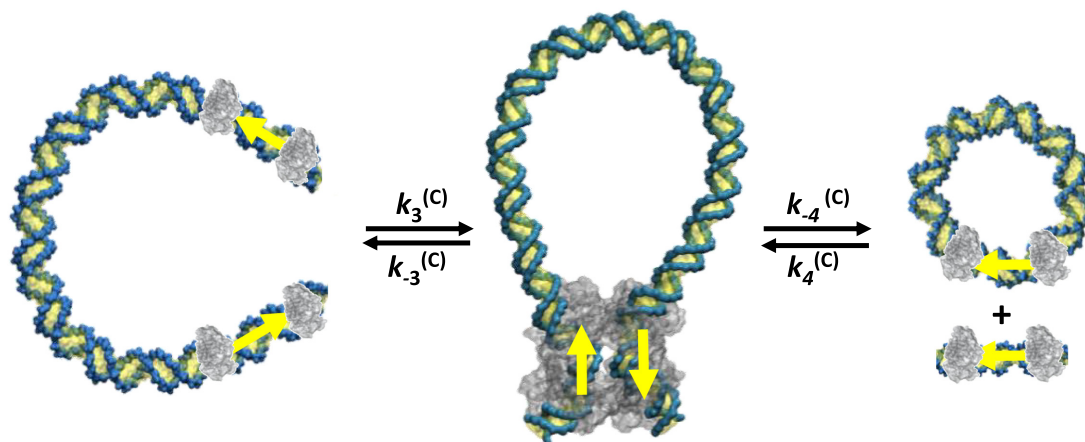
Figure 1. Products generated by Cre recombinase acting on the DNA molecules used in this study. In the first step DNA fragments flanked by directly repeated loxP sites (indicated by yellow arrows) form a DNA loop via site synapsis, which is mediated by a Cre-protein tetramer. Two sequential cleavage/strand-exchange events generate a short linear molecule and a DNA circle as recombinant products in the second step.

DNA polymerase and dNTPs from New England Biolabs (Ipswich, MA) (see Supplementary Figure S1). Excess primers were removed from the PCR products using NucleoSpin silica-membrane columns (Clontech, Mountain View, CA, USA) and the products were further purified in 3% agarose–TBE gels and subsequently reisolated using gel-purification kits (Clontech).

Protein purification

The expression vector for the His-tagged wild-type Cre_{WT} (pET28b-His6Cre) was a gift from Dr Enoch Baldwin at UC-Davis (22,26). The vector for the mutant Cre_{R101A} protein (pLC101A) was a gift from Dr Paul Sadowski at the University of Toronto (41). Both proteins were expressed from BL21(DE3) cells bearing the corresponding plasmids and were purified according to (42). Partially purified lysates were loaded onto equilibrated cobalt His-TALON columns (Clontech, Mountain View, CA, USA). The column was washed with 40–50 volumes of wash buffer (50 mM NaH_2PO_4, 300 mM NaCl, 10 mM imidazole; pH 7.8). The Cre protein was eluted using an imidazole gradient (10–150 mM). All of the eluted fractions were analyzed by Coomassie and $AgNO_3$-stained SDS-PAGE gels. The protein preparations were estimated to be over 90% homogenous. Cre-containing fractions were pooled and dialyzed against 20 mM Tris–Cl, 700 mM NaCl, 0.5 mM EDTA, 2 mM DTT and 0.05% (w/v) sodium azide; pH 7.8. Protein was concentrated using a centrifugal concentrator with an MWCO below 15 kDa (Millipore). The concentrated protein was sub-aliquoted, flash frozen and stored at $-80°C$.

FRET-based recombination-kinetics assays and analysis

Kinetics measurements were carried out using purified Cre_{WT} and Cre_{R101A} under conditions identical to the intramolecular-recombination assays described in (40). We employed numerical methods to extract rate constants for fundamental steps in the recombination pathway corresponding to synapse formation and dissociation. The modeled recombination pathways for both intermolecular and intramolecular recombination mechanisms and additional details of the curve-fitting procedure are also given in (40). Curve-fitting routines were implemented in MATLAB and used the functions *lsqcurvefit* for non-linear least-squares fitting and *ode15s* to solve the initial-value problem for the systems of ordinary differential equations. Analysis programs are available upon request (Figure 2).

Computational modeling of the looped synaptic complex

A Cre-bound DNA synapse is modeled as a chain of N rigid bodies labeled $k = 1, \ldots, N$. The terminal rigid bodies $k = 1, N$ represent Cre-bound loxP sites and correspond to half-tetramers in the Cre-loxP synapse. The remaining rigid bodies $k = 2, \ldots, N - 1$ represent single DNA base pairs spanning the Cre-bound loxP sites (Figure 3). The loop size, n, is the curvilinear distance in base pairs between centers of the flanking loxP sites; therefore, $N = n - 32$. Embedded within each rigid body is a body-fixed reference frame with positions and orientations, $\{\mathbf{r}^k, \mathbf{e}^k\}$. The boundary conditions for base pairs $k = 2, N - 1$ adjacent to the Cre-bound loxP sites are described by additional body-fixed auxiliary frames $\{\mathbf{r}'^1, \mathbf{e}'^1\}, \{\mathbf{r}'^N, \mathbf{e}'^N\}$, associated with the central DNA base pairs embedded within the Cre-bound loxP sites. The interaction between loxP sites in a Cre-mediated DNA loop is further described in terms of body-fixed auxiliary frames $\{\mathbf{r}''^1, \mathbf{e}''^1\}, \{\mathbf{r}''^N, \mathbf{e}''^N\}$ embedded in the loxP sites. The equilibrium shape (geometry) of the individual protein–DNA complexes and of the overall synaptic complex is fully characterized by the displacements of the auxiliary frames $\{\mathbf{r}'^k, \mathbf{e}'^k\}, \{\mathbf{r}''^k, \mathbf{e}''^k\}$ relative to the reference frames $\{\mathbf{r}^k, \mathbf{e}^k\}$ for $k = 1, N$. Conformations of the DNA segments within each half-tetramer were taken from the Cre synapse crystal structure 5CRX and held fixed (43).

The potential energy of a specific configuration of the Cre-bound DNA complex is given by

$$U = \frac{1}{2}(\mathbf{D} - \mathbf{D}_0)^T \mathbf{K} (\mathbf{D} - \mathbf{D}_0) \qquad (1)$$
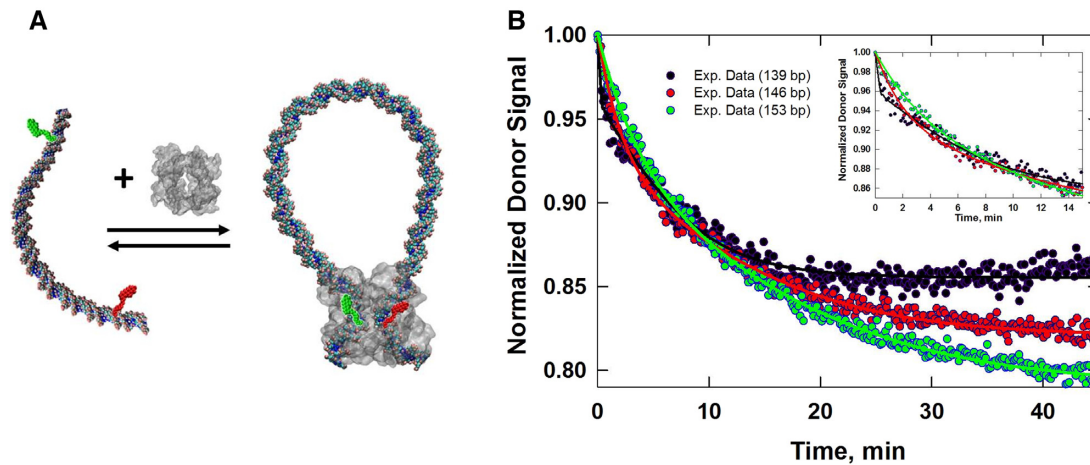
Figure 2. Intramolecular synapsis and recombination kinetics obtained from time-dependent FRET measurements. (**A**) Schematic of the intramolecular reaction carried out on a DNA fragment bearing donor- and acceptor-labeled loxP sites. (**B**) Donor-fluorescence signal, which monitors donor quenching via FRET during site synapsis and recombination. Fluorescence decays are shown for molecules having 139-, 146- and 153-bp DNA loops. Rate constants were obtained by fitting the fluorescence decay to a system of ordinary differential equations that describe the time-dependent concentrations of reactants, intermediates and products along the intramolecular recombination pathway (40). The best-fit numerical solution is given by the solid curve. The fluorescence decay and fit to the data over the first 15 minutes of the recombination reaction are shown in the inset.
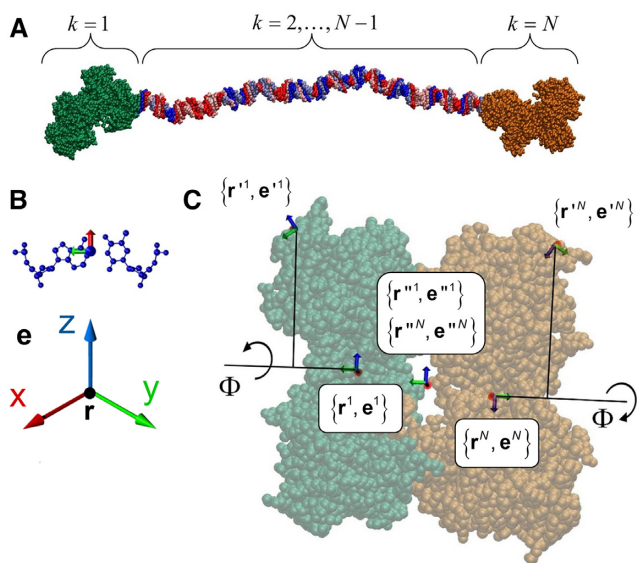

Figure 3. Nucleoprotein model. (**A**) DNA molecule with a pair of Cre-bound loxP sites at each end. The molecule shown is modeled as a chain of $N = 100$ rigid bodies. Each rigid body in the model is colored as follows: Cre-loxP protein-DNA complexes, green and orange; DNA base pairs: adenine (blue), thymine (light blue), cytosine (red), guanine (pink). (**B**) Definition of reference frames embedded within DNA base pairs: $\hat{e}_1$ axes (red) point toward the major groove, $\hat{e}_2$ axes (green) point toward the primary strand, and $\hat{e}_3$ axes (blue) point in the 5′ to 3′ direction of the sense strand. (**C**) Definition of the dihedral angle between Cre half tetramers in the synapse. The geometry of the Cre-loxP synaptic complex was modified from the nearly planar crystal structure geometry by applying rotations of the Cre-bound loxP sites as shown. Frame $\{\mathbf{r}'^1,\ \mathbf{e}'^1\}$ is rotated into the page by an angle Φ about the axis $\{\mathbf{r}^1,\ \hat{e}_2^1\}$ and frame $\{\mathbf{r}'^N,\ \mathbf{e}'^N\}$ is rotated out of the page by the same angle Φ about the axis $\{\mathbf{r}^N,\ \hat{e}_2^N\}$, increasing the dihedral angle of the loop ends in the protein synapse by 2Φ. For a definition of the body-fixed reference frames $\{\mathbf{r},\ \mathbf{e}\}$ see Materials and Methods, and an extended discussion of the synapse model in Supplementary Information.

where the vector $\mathbf{D}$ contains the $6N$ displacements between neighboring rigid bodies, $\mathbf{D}_0$ are the mechanical-equilibrium displacements for the linear form of the complex, and $\mathbf{K}$ is a $6N \times 6N$ stiffness matrix. Assuming only nearest-neighbor interactions, the displacement between any pair of frames k and $k+1$ is parameterized in terms of six local displacement coordinates (shift, slide, rise, tilt, roll, twist), which were calculated as detailed in (44). We took the helical parameters for $\mathbf{D}_0$ to be those of canonical B-form DNA with the exception of the twist (i.e. shift = slide = 0, rise = 0.34 nm, tilt = roll = 0, twist = $2\pi/h_0$ = 33.46° with $h_0 = 10.76$ bp turn^{-1}). A sequence-averaged stiffness matrix was obtained as $\mathbf{K} = \bar{\mathbf{C}}^{-1}$ where $\mathbf{C} = \mathbf{K}_s^{-1}$ is the covariance matrix of the stiffness matrix $\mathbf{K}_s$ obtained in (45) and the overbar denotes an average over the 10 independent base steps. Auxiliary frames $\{\mathbf{r}''^N,\ \mathbf{e}''^N\}$, $\{\mathbf{r}''^1,\ \mathbf{e}''^1\}$ were defined such that at mechanical equilibrium $\{\mathbf{r}''^N,\ \mathbf{e}''^N\} = \{\mathbf{r}''^1,\ \mathbf{e}''^1\}$, i.e. $\mathbf{D}_0^N = 0$. The stretching and rotational flexibility between the Cre-bound loxP sites was described by force constants k_s and k_r, respectively. We used $k_s = 5\ k_BT\cdot\text{Å}^{-2}$ and k_r was determined from fitting the model to experimental values of the J factor.

Initial positions and orientations of rigid bodies $k = 1, N$ describing Cre-bound loxP sites were obtained from the Protein Data Bank (PDB) for the Cre-loxP synaptic complex (PDB ID 5CRX). Coordinates of auxiliary frames $\{\mathbf{r}'^1,\ \mathbf{e}'^1\}$, $\{\mathbf{r}'^N,\ \mathbf{e}'^N\}$ were deduced using the software package 3DNA (46), and coordinates of auxiliary frames $\{\mathbf{r}''^1,\ \mathbf{e}''^1\}$, $\{\mathbf{r}''^N,\ \mathbf{e}''^N\}$ were obtained from the crystal structure of the complete synaptic complex (2 loxP + Cre tetramer). The Cre-loxP half tetramers, corresponding to two Cre monomers bound to a single loxP site, are relatively rigid structures (36), which we treat here as a single, rigid body connected by semi-flexible virtual chain segments to the opposing half tetramer and the remaining base-pair segments of the DNA chain. Therefore, the relative orientation of bound loxP half sites in a recombinase-DNA com-

plex is described by three rotations about perpendicular axes corresponding to twist, roll, and tilt, the latter changing the dihedral angle 2Φ between the loxP half sites. To study the deviation from planar-intermediate geometry of the Cre-bound loxP sites, the geometry was allowed to vary via the single rotational degree of freedom Φ, with associated energy constant k_r, while twist and roll angles were set to their equilibrium value zero (Figure 3). Thus, frame $\{\mathbf{r}'^1, \mathbf{e}'^1\}$ was permitted to rotate by an angle $\pm\Phi$ about the axis $\{\mathbf{r}^1, \hat{\mathbf{e}}_2^1\}$ and frame $\{\mathbf{r}'^N, \mathbf{e}'^N\}$ was rotated by the same angle $\pm\Phi$ about the axis $\{\mathbf{r}^N, \hat{\mathbf{e}}_2^N\}$. These rotations therefore increase the dihedral angle of the Cre-mediated loop at the protein synapse by 2Φ. By convention, a positive rotation of angle 2Φ corresponds to a right-handed crossing of the loxP sites. Note that these geometric constraints do not permit re-equilibration of DNA twist within DNA segments that make local protein–DNA contacts. Allowing such twist changes would strongly perturb the rotational register of Cre monomers in the synaptic complex, which would create entirely new sets of contacts. We regard such radical remodeling of local protein–DNA interactions as implausible.

Minimum-energy configurations of a Cre-bound DNA complex were obtained by using unconstrained minimization of the potential energy U in equation (1) using a trust-region normal-mode analysis (NMA) as described in (38,39). Theoretical J factors were calculated as the ratio $J = K_c/K_b$ of intramolecular and bimolecular equilibrium constants using a generalization of the NMA method in (48). In particular, K_b was calculated by applying NMA to a pair of bound and unbound rigid bodies describing Cre-bound loxP sites in the absence of an intervening DNA loop. J values were calculated for each minimum-energy configuration having preferred (lowest energy) linking number Lk_0. J factors for topoisomers with $Lk = Lk_0 \pm 1, 2, \ldots$ were approximated by fitting calculated J-factors with preferred linking number Lk_0 to the function $f(x) = \exp[-c_2(x - c_1)^2 + c_2]$ and extrapolating beyond Lk_0. Final J-factor values, accounting for multiple topoisomers, were calculated by summing J for all linking numbers. For illustration, J-factors calculated for a Cre-mediated DNA loop are shown in Supplementary Figure S2 for a range of DNA loop lengths 120–164 base pairs, using $k_s = 5 \, k_B T \cdot \text{Å}^{-2}$, $k_r = 5 \, k_B T \cdot \text{rad}^{-2}$, and DNA parameters $\mathbf{D}_0$, $\mathbf{K}$ described above. The equilibrium protein geometry was generated from the crystallographic structure of the Cre-loxP synaptic complex (PDB: 5CRX) (43).

RESULTS

Our presentation of the results is organized as follows: We first review the procedure employed to extract experimental J-factor values from kinetic data (originally described in (40)). Next, we present an independent topological measurement of the DNA helical repeat under the solution conditions used in the recombination kinetic experiments. We justify this procedure by demonstrating that it is not otherwise possible to uniquely determine the dihedral angular displacement of Cre half tetramers in the synaptic complex. The final Results section describes how the experimental J-factor data were fitted to our NMA-based statistical–mechanical model in order to generate solutions for the

adjustable elasto-mechanical parameters of a looped Cre-DNA synaptic complex.

Determining loop-closure probabilities from kinetic data

Independent measurements of inter- and intramolecular recombination rates permit quantitative determination of the probability of loop formation, J. Formally, J is a quotient of rate constants for intra- and intermolecular synapsis, given by

$$J = \frac{K^{(c)}}{K^{(b)}} = \frac{k_3^{(c)} k_{-3}^{(b)}}{k_{-3}^{(c)} k_3^{(b)}} \tag{2}$$

where each of the k_3/k_{-3} ratios pertains to corresponding apparent forward and reverse synapsis steps for the loop-closure and bimolecular synapsis reactions (superscripts $^{(c)}$ and $^{(b)}$, respectively) (40). Numerical values of the rate constants are fitted parameters in a system of ordinary differential equations evaluated from the time-dependent quenching of a FRET donor signal during the Cre reaction (40).

An additional challenge of J-factor measurements comes from the observation that inter- and intramolecular reactions generally do not take place under identical conditions. The limited range of intermolecular-recombination conditions is similar to that encountered in ligase-catalyzed bimolecular-joining reactions (22), which require higher concentrations of DNA substrate than for the corresponding intramolecular reaction. Failing to take possible dependencies on substrate or enzyme concentration into account can lead to large errors in $K^{(b)}$, and hence in the absolute value of J. The most rigorous approach for obtaining absolute measurements of J is to determine individual pairs of apparent rate constants for the intra- and intermolecular reactions under identical solution conditions, extrapolating to intramolecular reaction conditions where necessary. J factors for Cre-mediated looping of loxP sites separated by >800 bp have been determined using this method (40).

In Table 1 we report the J values for DNA loops of size $n = 130$–153 bp (taken as curvilinear distances in base pairs between the centers of directly repeated loxP sites) using the wild-type enzyme. Recombination of the directly repeated loxPs is a deletion reaction that generates a small, circular recombination product whose size in base pairs is exactly equal to that of the Cre-mediated loop along with a 34-bp linear product (Figure 1). The recombination substrates were designed with internal donor- and acceptor-fluorophore labels located within the spacer regions of loxP sites, which are positioned near the ends of the molecules (see Supplementary Figure S1). In order to prevent the formation of intermolecular-recombination products, kinetic assays were carried out at bulk loxP concentrations not exceeding 0.5 nM, an order of magnitude below the target-site bulk-concentration threshold for intermolecular Cre recombination (40). Post-hoc analysis of the reactions by agarose-gel electrophoresis also confirmed that the yield of intermolecular-recombination products was negligible under our conditions (as shown in (40)).

Figure 2 shows that excellent fits are obtained for the time-dependent FRET signals to ordinary-differential

Table 1. J-factor values and uncertainties expressed as standard deviations, J_{err}. Each data point is the average of at least five independent measurements

Loop size (n), bp	J_{exp}, nM	J_{err}, nM
131	1.1	0.5
133	2.5	0.2
134	6.4	0.2
135	7.9	0.3
137	17.1	0.3
138	14.8	0.4
139	10.6	0.3
140	2.9	0.4
142	2.2	0.3
143	2.7	0.3
144	4.8	0.4
145	14.0	0.3
146	18.5	0.2
147	19.4	0.2
148	18.7	0.3
149	13.5	0.3
151	7.2	0.4

equation (ODE) solutions for the intramolecular single-intermediate Cre-recombination pathway (40). Different plateau FRET values are observed for these constructs and stronger FRET signals are qualitatively expected for molecules that form more thermodynamically favored looped structures, *i.e.*, loops having larger values of *J*. However, *J* is a thermodynamic quantity and not directly obtained from the steady-state FRET-signal amplitude. The observed FRET signal is, in fact, a weighted superposition of FRET amplitudes attributable to donor fluorophores in the synaptic complex as well as in the recombinant product. We account for this by using a fixed parameter in the fitting routine corresponding to the steady-state quenching of donor fluorescence upon synapsis of the donor- and acceptor-labeled loxP sites. This quenching is quantified by the ratio of donor quantum yields in the Cre synaptosome to that for the Cre-bound donor-labeled substrate alone, $\phi = \phi_{sc}^{DA}/\phi_{sc}^{D}$, and was taken to be 0.12, a value determined previously for intermolecular synapsis (40).

The rate constants $k_3^{(c)}$, $k_{-3}^{(c)}$, $k_4^{(c)}$, $k_{-4}^{(c)}$, which appear in the system of ODEs modeling the recombination mechanism, were treated as adjustable parameters. Remaining rate constants were fixed at the same values used in previous studies (40,47). As shown in Figure 2, the overall amplitude of the FRET signal varied significantly with loop size, asymptotically approaching decreases of between 10 and 25 percent over the course of 45-minute reactions.

Measurements of DNA helical repeat under recombination-reaction conditions

J as a function of the loop size *n* is a periodic function, whose amplitude, offset, and phase are not single-valued with respect to synapse geometry. In particular, interpreting the measured *J*(*n*) values in terms of a geometric model of the Cre-loxP synapse depends strongly on the DNA helical repeat, h_0. Both small changes in synapse geometry and h_0 can lead to pronounced shifts in the theoretical dependence of *J* on loop size; indeed, accurate solutions for the geometric variables that describe the conformation of the protein-

DNA synapse cannot be obtained in general without measuring h_0, as discussed below. Additional uncertainties in h_0 can arise in cases where unusual buffer conditions are employed. In this study, particular buffer conditions were used that (i) reproduce the conditions used in previous measurements of apparent Cre-loxP reaction rate constants, values of which are needed in order to solve the system of ODEs that describes the reaction pathway (40); (ii) allow for determination of synapsis rate constants for both looping and bimolecular joining under closely similar conditions (47).

We note that possible effects of solution conditions are rarely considered or independently measured despite the established fact that counterion type and concentration measurably affect DNA helical repeat (48), as do non-aqueous solvents that have strong effects on water activity. The requisite recombination-reaction solution conditions (40,47) contain significant concentrations of polyethylene glycol (PEG) and glycerol (10% and 20% (w/v), respectively). Previous studies of effects of 'dehydrating agents' on DNA twist showed that glycerol, as well as other non-aqueous solvents such as ethylene glycol and dimethyl sulfoxide, increase the DNA helical repeat in the range of non-aqueous solvent concentrations used in our study (49). We therefore carried out independent measurements of the DNA helical repeat for this series of loxP substrates under our recombination-reaction conditions.

Helical-repeat values were measured using a technique developed in our laboratory that is based on the dependence of gel-electrophoretic mobility on plasmid size for individual DNA topoisomers (9). The mobilities of topoisomers resolved in one-dimensional electrophoresis experiments vary discontinuously at critical values of the construct size, leading to a saw-tooth dependence on plasmid size that is highly sensitive to the helical repeat of the variable-size region. By fitting this size dependence to parameters that affect the writhe of superhelical molecules, including the torsional and bending persistence lengths of the DNA, we found that the most-probable helical-repeat value for the looped DNA segment in our recombination buffer is 10.76 ($\pm$0.05) bp turn^{-1}, a significant departure from the canonical value of 10.45 bp turn^{-1} (50). (Supplementary Figure S3). Uncertainties in fitted parameters from this analysis were estimated by a bootstrap resampling procedure, and are similar to values obtained from similar analyses using this technique (9). Supplementary Figure S3b shows expected dependencies of topoisomer mobility on DNA size for $h_0 =$ 10.45 and 11.0 bp turn^{-1} to underscore the fact that neither of these values is consistent with a fit to the topoisomer-mobility data.

Fitting the experimental values of *J* to a structural model of the Cre-loxP synaptosome

In a previous analysis of lac repressor-operator complexes we used the helical dependence of gene repression over short curvilinear operator-operator distances to determine the most-probable geometry of the lac-repressor tetramer (51). The theory used to fit those data was based on a semi-analytical harmonic approximation to the free energy of DNA looping (37). Here, we employ an extension of this approach based on normal-mode analysis (NMA) to fit a

structural model of the Cre-loxP synaptosome to the experimentally measured J-factor values, $J_{exp}(n)$, where n is the number of base pairs in the Cre-loxP mediated DNA loop. NMA allows one to calculate the free energy and to identify the principal modes of vibration of macromolecular structures fluctuating about a mechanical-energy minimum and is mathematically equivalent to the harmonic approximation (38,39).

The present structural model of the Cre-loxP synaptosome regards the looped nucleoprotein complex as a Cre half-tetramer anchoring the base of a DNA loop n base pairs in size. DNA base pairs and individual Cre subunits are treated as a connected set of rigid bodies as described in (37) and (44). Whereas DNA base pairs and loxP-bound Cre monomers are treated as rigid entities, their respective interactions with adjacent base pairs and neighboring protein subunits are governed by purely harmonic potential energies (see Figure 3 and Methods).

A systematic grid search of J-factor dependence on DNA conformational variables in the HJ-containing synaptic complex indicated that the helical dependence of J is highly sensitive to the dihedral half angle, Φ, and largely insensitive to other parameters, such as the half-tetramer inter-arm angle. Therefore, to fit the computed J-factor curves to the experimental J-factor values we took both the dihedral half-angle Φ subtended by the Cre monomers (Figure 3) and an associated elastic-energy constant k_r (in units of $k_B T \cdot \text{rad}^{-2}$) as adjustable parameters. Figure 4A shows the 2D map of residuals

$$\chi^2 = \frac{1}{n} \sum_n \left\{ a + \log\left[J_{\text{NMA}}(n)\right] - \log\left[J_{exp}(n)\right] \right\}^2 \quad (3)$$

as a function of Φ and k_r for wild-type Cre-mediated looping. In this calculation we optimized the parameter a in equation (3) to minimize χ^2 for each pair of values (Φ, k_r). This procedure is justified as follows. Using the general method for computing conformational free energies of DNA tertiary structures and nucleoprotein assemblies developed in (38) we found that for DNA molecules on the length scale considered here ($\approx$200 bp) the deviation of the free energy computed by NMA alone from exact values is of the order of the thermal energy, $k_B T$ (where k_B is the Boltzmann constant and $T = 300$ K is the temperature) (39). The parameter a in equation (3) accounts for this deviation, and is expected to depend on the values (Φ, k_r), but not on the loop size n for the range of loop sizes considered here. The fact that the optimal values of a in equation (2), corresponding to an offset in free energy $\log[J_{\text{NMA}}(n)]$ in units of $k_B T$, are indeed of order 1 shows that the procedure is consistent (Supplementary Figure S5). Note that a variation of the parameter a in equation (3) amounts to shifting computed J-factor curves $\log[J_{\text{comp}}(n)] \equiv a + \log[J_{\text{NMA}}(n)]$ vertically up and down, and therefore does not affect the optimal angle Φ which is essentially determined by adjusting the *phase* of the computed J-factor curves to the measured J-factor values (Figure 4B). The DNA properties used in the calculation of $J_{\text{NMA}}(n)$ were based on uniform (non-sequence-dependent) helico-elastic parameters, including the measured sequence-averaged helical repeat of 10.76 bp turn^{-1} reported above. The χ^2 plot exhibits a clear
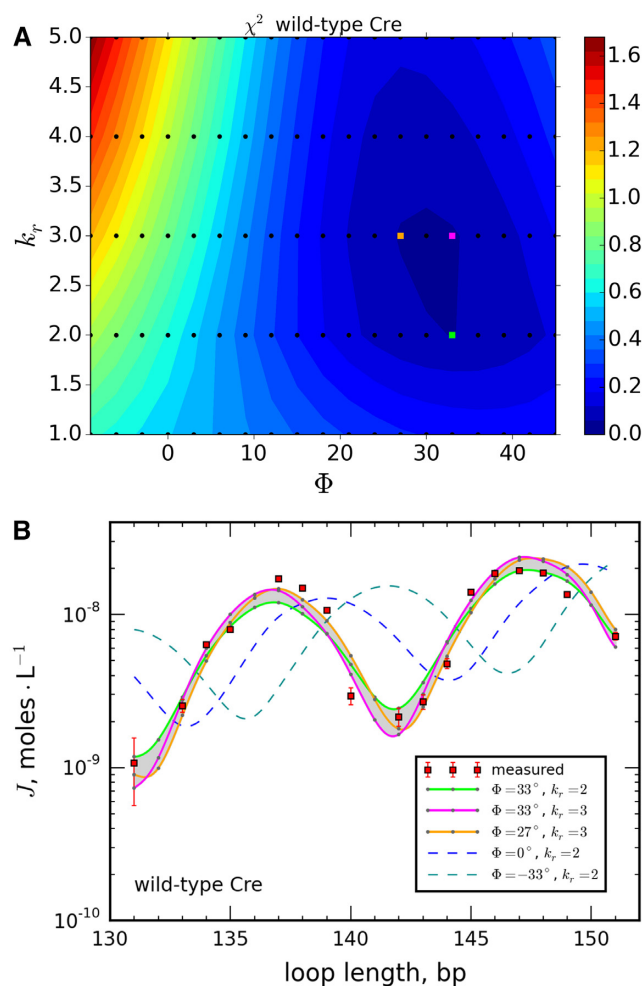
Figure 4. Contour map of solutions and optimal fits of calculated J-factor curves to measured J-factor values for wild-type Cre-mediated looping. (**A**) Contour plots of the mean-square error, *MSE*, for fitting of experimental J factors to NMA-computed values for the wild-type Cre synapse as a function of the dihedral angle Φ and rotational flexibility constant k_r for the pair of Cre half-tetramers (see Methods). (**B**) Measured values of J for wild-type Cre along with an envelope of optimally fitted J-factor curves, corresponding to values (Φ, k_r) indicated by the three highlighted points in the contour map shown in (**A**). Each data point is the average of at least three independent measurements and error bars indicate ±1 standard error. The envelope of optimal Φ values spans the range 27° (orange)$\leq \Phi \leq$33° (green) with $2 \leq k_r \leq 3$ $k_B T \cdot \text{rad}^{-2}$. A particular solution in this range for $\Phi = 33°$ with $k_r = 3$ $k_B T \cdot \text{rad}^{-2}$ is shown in magenta. Calculated J-factor curves for $\Phi = 0°$ (blue dashed curve) and $\Phi = -33°$ (cyan dashed curve) with $k_r = 2$ $k_B T \cdot \text{rad}^{-2}$, provided for comparison, do not provide satisfactory fits to the experimental data.

minimum at $\Phi = 33°$ and $k_r = 2.5 k_B T$ rad^{-2} (Figure 4A). Figure 4B shows experimental J-values, $J_{\text{exp}}(n)$, along with computed J-factor curves $J_{\text{comp}}(n)$ corresponding to the envelope of optimal Φ and k_r values: $+27° \leq \Phi \leq +33°$ and $2k_B T$ rad$^{-2} \leq k_r \leq 3k_B T$ rad^{-2}. In contrast, the helical dependence of $J_{\text{comp}}(n)$ for $\Phi = 0°$ and $\Phi = -33°$ (achiral planar and left-handed geometries, respectively) shown in Figure 4B do not provide satisfactory fits to the experimental data. Figure 5 shows a 3D model of the fitted structure of the synaptic complex (also see Supplementary Animation 1).
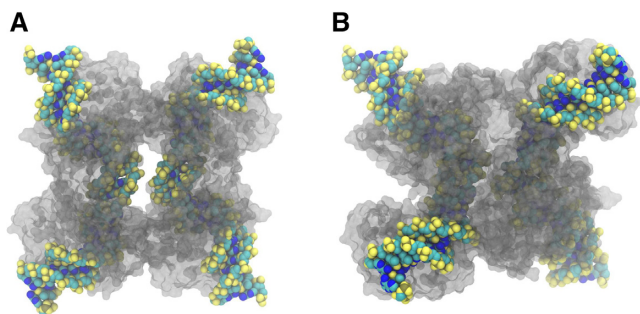
A **B**

Figure 5. 3D models of Cre synaptic complexes according to (**A**) crystal structure 5CRX and (**B**) minimum-elastic energy structure corresponding to the optimum fit of the NMA model to our experimental J-factor data.

The computed J-factor curves and optimal value of Φ shown in Figure 4B depend strongly on the value of the helical repeat h_0 used in the model. The value $h_0 = 10.76 \pm 0.05$ bp turn^{-1} used in Figure 4B was determined experimentally for the buffer conditions present in this study (Section Measurement of DNA helical repeat under recombination-reaction conditions and Supplementary Figure S3). Variations in h_0 generate closely similar optimal J-factor curves, but are consistent with sharply different optimal values of Φ (Supplementary Figure S4). Therefore, an accurate and independent determination of h_0 is required to obtain reliable predictions for Φ.

DISCUSSION

Although our theoretical understanding of DNA-loop formation (and DNA cyclization as a special case) has progressed over more than twenty-five years, there has been a lag in applying the theory to analyses of experimental data. One possible barrier to wider use of loop-closure kinetics in solution is a scarcity of methods for monitoring the kinetics of loop formation with adequate temporal resolution to provide reliable values of rate constants. Here we employ a FRET-based measurement of recombination-site synapsis at sufficient temporal resolution to investigate the intramolecular synapsis of two loxP sites tethered by short ($\lesssim$ one persistence length) DNA segments. The use of small looped DNAs in such assays allows the geometry of the looped recombinase-DNA complex to be determined from *J*-factor measurements with high sensitivity. This approach can be a valuable complement to the analysis of nucleoprotein assemblies by topological methods, which generally remain ambiguous with respect to geometric details.

Here, we focus on a particular asymmetry in the synaptic complexes of tyrosine site-specific DNA recombinases (λ Int, Cre, and Flp). A previous topological study of tyrosine recombinases, including Cre, revealed an excess of (+)-noded knotted recombinant DNA products over (–)-noded topologies (29). This excess implies the existence of a productive right-handed recombination intermediate; however, no available crystallographic structure for any of these recombinases with their DNA target sites shows significant right-handed chirality. The data presented here provide the first direct evidence for a right-handed recombination intermediate in solution and also support apparent asymmetries in the arrangement of recombination sites observed by atomic-force and electron microscopy (30,52). It is difficult to conceive of a mechanism whereby product chirality arises from solely non-productive conformational preferences. Therefore, we conclude that the chiral intermediate described here likely has an active role in the recombination pathway.

Our method considers the dynamic behavior of Cre synaptic complexes rather than a single static, or average, structure. An inherent characteristic of ensemble-based kinetic methods is that they typically probe only the intermediate species with the longest lifetime. Thus, it is possible that other synapse geometries with shorter lifetimes, including achiral crystallographic structures, may exist along the recombination pathway. A single-molecule FRET analysis based on various crystallographic synaptic complexes identified a subset of possible intermediate conformations that may characterize distinct steps in the recombination pathway (33). Due to the inherent difficulties of obtaining absolute distance measurements from FRET-efficiency values (40,53,54), it is difficult to assign a particular geometry to the observed intermediates and the possibility of one or more productive non-planar intermediate structures should not be completely ruled out.

Finally, to resolve potential roles of specific mechanistic steps in the Cre-recombination pathway, we analyzed the loop-closure kinetics for a subset of loxP substrates using a mutant form of Cre (R101A), which is defective in isomerization and resolution of the central Holliday-junction intermediate. We chose this particular Cre mutant in order to ascertain whether the chiral bias is a feature of intermediate structures generated during early or later steps in the recombination pathway. The R101A mutant is known to block middle-to-late stages of the pathway but does not inhibit the formation of the HJ intermediate (41). In previous work, we have shown, using a cleavage-deficient mutant of the mechanistically similar recombinase Flp (52), that a conformational bias in synaptic-complex geometry requires initial formation of an HJ intermediate.

Loop-closure kinetics data for the R101A mutant show that this synapse is also right-handed with a somewhat larger dihedral angle ($\Phi \approx 45°$) relative to the wild-type complex (Figure 6). Therefore, inhibiting the isomerization/resolution of the central HJ intermediate leads to a somewhat larger dihedral half angle, Φ. In the wild-type reaction we speculate that, if there is sufficiently rapid averaging of a structure with a larger Φ value at the isomerization step together with a structure that is less chirally biased (e.g. $\Phi \approx 0$), this could explain the overall smaller value of Φ (33°) measured for the wild-type recombinase.

We note that the apparent experimental J-factor values for the R101A mutant are higher than those measured for Cre$_{WT}$. This can be explained in terms of the implicit assumption that the values of K_b are similar for the mutant and wild-type enzymes (see Equation 2). We had previously measured K_b for Cre$_{WT}$ (40), however, for technical reasons we did not redetermine this parameter for Cre$_{R101A}$. Errors in K_b for the mutant Cre can yield a systematic shift (up or down) in the apparent values of *J*. However, this does not affect the phasing of the *J*-factor loop-size dependence
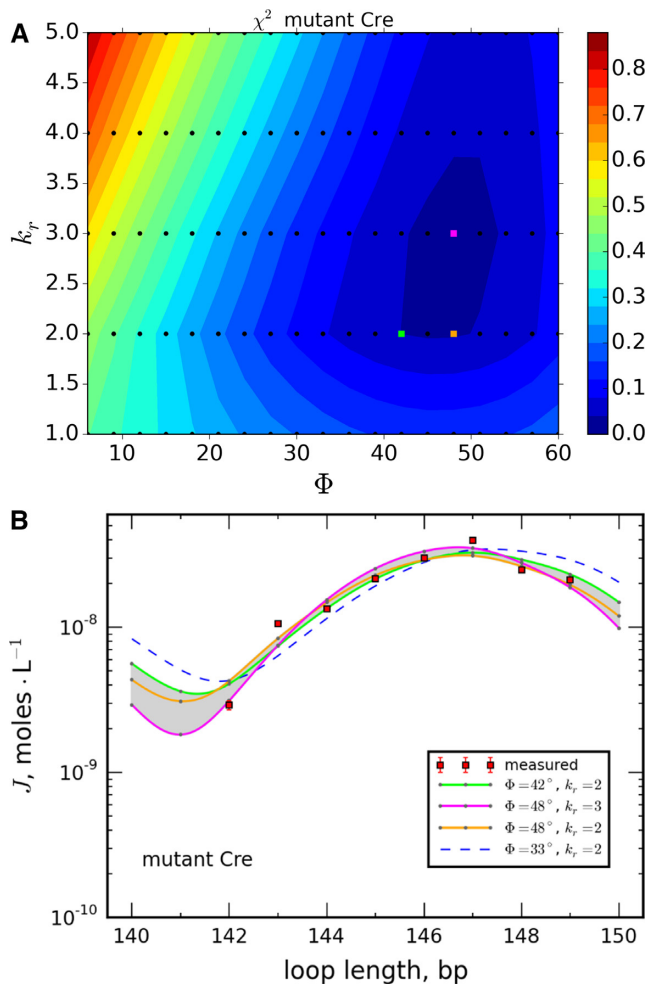
Figure 6. Contour map of solutions and optimal fits of calculated J-factor curves to measured J-factor values for Cre-mediated looping by the R101A mutant Cre protein. The R101A mutation strongly reduces the protein's Holliday-junction resolution activity, promoting the accumulation of junction-containing synaptic complexes. Contour plots (**A**) and optimally fitted *J*-factor curves (**B**) for mutant Cre were obtained as described in Figure 4. Optimal fits were obtained for $42° \leq \Phi \leq 48°$ (green) and $k_r = 2 \, k_B T \cdot \mathrm{rad}^{-2}$. A particular solution for $\Phi = 48°$ with $k_r = 3 \, k_B T \cdot \mathrm{rad}^{-2}$ is also shown in magenta. The *J*-factor dependence for $\Phi = 33°$ and $k_r = 2 \, k_B T \cdot \mathrm{rad}^{-2}$, which lies within the best-fit envelope of the wild-type protein, is shown for comparison (blue dashed curve).

and hence has no effect on the fitted value of Φ as noted above. The important conclusion to be drawn from Figures 4 and 6 is that there is a significant difference in helical phasing between the wild-type and mutant synapses and thus different optimal values of Φ and k_r.

The existence of a stable conformational intermediate with significant right-handed chirality leads to symmetry breaking in the distribution of recombination-product topologies (Figure 5). It may also reflect biological asymmetries that arise from the right-handed geometry of the DNA double helix. Packing of DNA helices at high densities, such as in some crystal structures (55–57), have biases for right-handed configurations that are sterically favorable due to reciprocal fitting of the DNA backbone and duplex major groove. Right-handed duplex geometry also contributes to

the chiral organization of DNA in viral capsids (58) and some liquid-crystalline phases (59,60). Finally, crystal structures of isolated HJs (in the absence of junction-binding proteins) seem to invariably adopt right-handed 'stacked-X' structures with interduplex angles comparable to the values measured in this work (61,62). The consensus view is that HJs are highly dynamic entities, a conclusion that is supported by the kinetic analysis presented here.

Beyond applications to site-specific recombination systems, loop-closure kinetics measurements are a potentially powerful technique for characterizing the geometry of complex multi-protein assemblies interacting with DNA and chromatin. One application that should be explored is the use of this kinetic loop-closure assays in combination with HiC Chromatin Immunoprecipitation (Hi-ChIP) (63). Adapted to a high-throughput format, such kinetic assays could address conformational details and give information about the dynamics of nucleoprotein complexes that remain inaccessible to atomic-resolution methods. Finally, we note that biophysical insights into general mechanisms of endogenous circular-DNA excision and re-integration are important for understanding extrachromosomal circular-DNA (eccDNA) biogenesis and dynamics (64–73). New techniques, such as that described here, can work in concert with genomic tools to reveal the thermodynamic and kinetic principles that underlie the organization of the 4D genome (74).

SUPPLEMENTARY DATA

Supplementary Data are available at NAR Online.

REFERENCES

1. Castán,A., Hernández,P., Krimer,D.B. and Schvartzman,J.B. (2018) DNA catenation reveals the dynamics of DNA topology during replication. In: Drolet,M (ed). *DNA Topoisomerases: Methods and Protocols*. Springer New York, NY, pp. 75–86.

2. Keszthelyi,A., Minchell,N.E. and Baxter,J. (2016) The causes and consequences of topological stress during DNA replication. *Genes (Basel)*, **7**, 134.

3. Dorman,C.J. and Dorman,M.J. (2016) DNA supercoiling is a fundamental regulatory principle in the control of bacterial gene expression. *Biophys. Rev.*, **8**, 209–220.

4. Racko,D., Benedetti,F., Dorier,J., Burnier,Y. and Stasiak,A. (2015) Generation of supercoils in nicked and gapped DNA drives DNA unknotting and postreplicative decatenation. *Nucleic Acids Res.*, **43**, 7229–7236.

5. Rice,P.A. (2015) Serine resolvases. *Microbiol Spectr*, **3**, doi:10.1128/microbiolspec.MDNA3-0045-2014.

6. Kouzine,F., Levens,D. and Baranello,L. (2014) DNA topology and transcription. *Nucl. (United States)*, **5**, 195–202.

7. Sherratt,D.J., West,S.C., Hardy,C.D., Crisona,N.J., Stone,M.D. and Cozzarelli,N.R. (2004) Disentangling DNA during replication: a tale of two strands. *Philos. Trans. R. Soc. London. Ser. B Biol. Sci.*, **359**, 39–47.

8. Martínez-García,B., Valdés,A., Segura,J., Dyson,S., Díaz-Ingelmo,O. and Roca,J. (2018) Electrophoretic analysis of the DNA supercoiling activity of DNA gyrase. In: Lavelle,C (ed). *Molecular Motors: Methods and Protocols*. Springer New York, NY, pp. 291–300.

9. Vetcher,A.A., McEwen,A.E., Abujarour,R., Hanke,A. and Levene,S.D. (2010) Gel mobilities of linking-number topoisomers and their dependence on DNA helical repeat and elasticity. *Biophys. Chem.*, **148**, 104–111.

10. Levene,S.D. (2009) Analysis of DNA topoisomers, knots, and catenanes by agarose Gel electrophoresis. In: Clarke,DJ (ed). *DNA Topoisomerases: Methods and Protocols*. Humana Press, Totowa, pp. 11–25.

11. Shimokawa,K., Ishihara,K., Grainge,I., Sherratt,D.J. and Vazquez,M. (2013) FtsK-dependent XerCD-dif recombination unlinks replication catenanes in a stepwise manner. *Proc. Natl. Acad. Sci. U.S.A.*, **110**, 20906–20911.

12. Darcy,I.K. and Vazquez,M. (2013) Determining the topology of stable protein–DNA complexes. *Biochem. Soc. Trans.*, **41**, 601–605.

13. Amin,S., Khorshid,A., Zeng,L., Zimny,P. and Reisner,W. (2018) A nanofluidic knot factory based on compression of single DNA in nanochannels. *Nat. Commun.*, **9**,1506–1516.

14. Liu,D., Chen,G., Akhter,U., Cronin,T.M. and Weizmann,Y. (2016) Creating complex molecular topologies by configuring DNA four-way junctions. *Nat. Chem.*, **8**, 907–914.

15. Seeman,N.C. (1998) DNA nanotechnology: novel DNA constructions. *Annu. Rev. Biophys. Biomol. Struct.*, **27**, 225–248.

16. Jones,J.R., Shelton,K.D. and Magnuson,M.A. (2005) Strategies for the use of site-specific recombinases in genome engineering. *Methods Mol. Med.*, **103**, 245–257.

17. Van Houdt,R., Leplae,R., Lima-Mendez,G., Mergeay,M. and Toussaint,A. (2012) Towards a more accurate annotation of tyrosine-based site-specific recombinases in bacterial genomes. *Mob. DNA*, **3**, 1–11.

18. Van Duyne,G.D. (2005) Lambda integrase: armed for recombination. *Curr. Biol.*, **15**, R658–R660.

19. Austin,S., Ziese,M. and Sternberg,N. (1981) A novel role for site-specific recombination in maintenance of bacterial replicons. *Cell*, **25**, 729–736.

20. Van Duyne,G.D. (2015) Cre recombinase. *Microbiol. Spectr.*, **3**, 1–19.

21. Champoux,J.J. (1990) Mechanistic aspects of type-I DNA topoisomerases. In: *Cold Spring Harbor Monograph Archive; Volume 20 (1990): DNA Topology and Its Biological Effects*. Vol. **20**, pp. 217–242.

22. Martin,S.S., Pulido,E., Chu,V.C., Lechner,T.S. and Baldwin,E.P. (2002) The order of strand exchanges in Cre-LoxP recombination and its basis suggested by the crystal structure of a Cre-LoxP Holliday junction complex. *J. Mol. Biol.*, **319**, 107–127.

23. Guo,F., Gopaul,D.N. and van Duyne,G.D. (1997) Structure of Cre recombinase complexed with DNA in a site-specific recombination synapse. *Nature*, **389**, 40–46.

24. Gopaul,D.N., Guo,F. and Van Duyne,G.D. (1998) Structure of the Holliday junction intermediate in Cre-loxP site- specific recombination. *EMBO J.*, **17**, 4175–4187.

25. Ennifar,E., Meyer,J.E., Buchholz,F., Stewart,A.F. and Suck,D. (2003) Crystal structure of a wild-type Cre recombinase-loxP synapse reveals a novel spacer conformation suggesting an alternative mechanism for DNA cleavage activation. *Nucleic Acids Res.*, **31**, 5449–5460.

26. Gelato,K.A., Martin,S.S. and Baldwin,E.P. (2005) Reversed DNA strand cleavage specificity in initiation of Cre-LoxP recombination induced by the His289Ala active-site substitution. *J. Mol. Biol.*, **354**, 233–245.

27. Ghosh,K. and Van Duyne,G.D. (2002) Cre-loxP biochemistry. *Methods*, **28**, 374–383.

28. Van Duyne,G.D. (2001) A structural view of Cre-loxP site-specific recombination. *Annu. Rev. Biophys. Biomol. Struct.*, **30**, 87–104.

29. Crisona,N.J., Weinberg,R.L., Peter,B.J., Sumners,D.W. and Cozzarelli,N.R. (1999) The topological mechanism of phage lambda integrase. *J. Mol. Biol.*, **289**, 747–775.

30. Vetcher,A.A., Lushnikov,A.Y., Navarra-Madsen,J., Scharein,R.G., Lyubchenko,Y.L., Darcy,I.K. and Levene,S.D. (2006) DNA topology and geometry in Flp and Cre recombination. *J. Mol. Biol.*, **357**, 1089–1104.

31. Fan,H.F., Ma,C.H. and Jayaram,M. (2018) Single-molecule tethered particle motion: stepwise analyses of site-specific DNA recombination. *Micromachines*, **9**, 1–23.

32. Fan,H.G., Cheng,Y.S., Ma,C.H. and Jayaram,M. (2015) Single molecule TPM analysis of the catalytic pentad mutants of Cre and Flp site-specific recombinases: Contributions of the pentad residues to the pre-chemical steps of recombination. *Nucleic Acids Res.*, **43**, 3237–3255.

33. Pinkney,J.N., Zawadzki,P., Mazuryk,J., Arciszewska,L.K., Sherratt,D.J. and Kapanidis,A.N. (2012) Capturing reaction paths and intermediates in Cre-loxP recombination using single-molecule fluorescence. *Proc. Natl. Acad. Sci. U.S.A.*, **109**, 20871–20876.

34. Fan,H.F. (2012) Real-time single-molecule tethered particle motion experiments reveal the kinetics and mechanisms of Cre-mediated site-specific recombination. *Nucleic Acids Res.*, **40**, 6208–6222.

35. Roy,R., Hohng,S. and Ha,T. (2008) A practical guide to single-molecule FRET. *Nat. Methods*, **5**, 507.

36. Shoura,M.J., Ranatunga,R.J.K.U., Harris,S.A., Nielsen,S.O. and Levene,S.D. (2014) Contribution of fluorophore dynamics and solvation to resonant energy transfer in protein-DNA complexes: A molecular-dynamics study. *Biophys. J.*, **107**, 700–710.

37. Zhang,Y., McEwen,A.E., Crothers,D.M. and Levene,S.D. (2006) Statistical-mechanical theory of DNA looping. *Biophys. J.*, **90**, 1903–1912.

38. Giovan,S.M., Scharein,R.G., Hanke,A. and Levene,S.D. (2014) Free-energy calculations for semi-flexible macromolecules: Applications to DNA knotting and looping. *J. Chem. Phys.*, **141**, 174902.

39. Giovan,S.M., Hanke,A. and Levene,S.D. (2015) DNA cyclization and looping in the wormlike limit: normal modes and the validity of the harmonic approximation. *Biopolymers*, **103**, 528–538.

40. Shoura,M.J., Vetcher,A.A., Giovan,S.M., Bardai,F., Bharadwaj,A., Kesinger,M.R. and Levene,S.D. (2012) Measurements of DNA-loop formation via Cre-mediated recombination. *Nucleic Acids Res.*, **40**, 7452–7464.

41. Lee,L. and Sadowski,P.D. (2003) Identification of Cre residues involved in synapsis, isomerization, and catalysis. *J. Biol. Chem.*, **278**, 36905–36915.

42. Woods,K.C., Martin,S.S., Chu,V.C. and Baldwin,E.P. (2001) Quasi-equivalence in site-specific recombinase structure and function: crystal structure and activity of trimeric Cre recombinase bound to a three-way Lox DNA junction. *J. Mol. Biol.*, **313**, 49–69.

43. Guo,F., Gopaul,D.N. and Van Duyne,G.D. (1999) Asymmetric DNA bending in the Cre-loxP site-specific recombination synapse. *Proc. Natl. Acad. Sci. U.S.A.*, **96**, 7143–7148.

44. Lankas,F., Gonzalez,O., Heffler,L.M., Stoll,G., Moakher,M. and Maddocks,J.H. (2009) On the parameterization of rigid base and basepair models of DNA from molecular dynamics simulations. *Phys. Chem. Chem. Phys.*, **11**, 10565–10588.

45. Lankas,F., Sponer,J., Langowski,J. and Cheatham,T.E. (2003) DNA basepair step deformability inferred from molecular dynamics simulations. *Biophys. J.*, **85**, 2872–2883.

46. Lu,X.J. and Olson,W.K. (2003) 3DNA: A software package for the analysis, rebuilding and visualization of three-dimensional nucleic acid structures. *Nucleic Acids Res.*, **31**, 5108–5121.

47. Ringrose,L., Lounnas,V., Ehrlich,L., Buchholz,F., Wade,R. and Stewart,A.F. (1998) Comparative kinetic analysis of Flp and Cre

recombinases: mathematical models for DNA binding and recombination. *J. Mol. Biol.*, **284**, 363–384.

48. Bauer,W.R. (1978) Structure and reactions of closed duplex DNA. *Annu. Rev. Biophys. Bioeng.*, **7**, 287–313.

49. Lee,C.H., Mizusawa,H. and Kakefuda,T. (1981) Unwinding of double-stranded DNA helix by dehydration. *Proc. Natl. Acad. Sci. U.S.A.*, **78**, 2838–2842.

50. Crothers,D.M., Drak,J., Kahn,J.D. and Levene,S.D. (1992) DNA bending, flexibility, and helical repeat by cyclization kinetics. *Methods Enzymol.*, **212**, 3–29.

51. Zhang,Y., McEwen,A.E., Crothers,D.M. and Levene,S.D. (2006) Analysis of in-vivo LacR-mediated gene repression based on the mechanics of DNA looping. *PLoS One*, **1**, e136.

52. Huffman,K.E. and Levene,S.D. (1999) DNA-sequence asymmetry directs the alignment of recombination sites in the FLP synaptic complex. *J. Mol. Biol.*, **286**, 1–13.

53. VanBeek,D.B., Zwier,M.C., Shorb,J.M. and Krueger,B.P. (2007) Fretting about FRET: correlation between kappa and R. *Biophys. J.*, **92**, 4168–4178.

54. Munoz-Losa,A., Curutchet,C., Krueger,B.P., Hartsell,L.R. and Mennucci,B. (2009) Fretting about FRET: failure of the ideal dipole approximation. *Biophys. J.*, **96**, 4779–4788.

55. Timsit,Y. and Moras,D. (1991) Groove-backbone interaction in B-DNA. Implication for DNA condensation and recombination. *J. Mol. Biol.*, **221**, 919–940.

56. Timsit,Y. and Moras,D. (1994) DNA self-fitting: the double helix directs the geometry of its supramolecular assembly. *EMBO J.*, **13**, 2737–2746.

57. Timsit,Y. (2013) DNA self-assembly: From chirality to evolution. *Int. J. Mol. Sci.*, **14**, 8252–8270.

58. Arsuaga,J., Vazquez,M., McGuirk,P., Trigueros,S., Sumners,D.W. and Roca,J. (2005) DNA knots reveal a chiral organization of DNA in phage capsids. *Proc. Natl. Acad. Sci. U.S.A.*, **102**, 9165–9169.

59. Mitov,M. (2017) Cholesteric liquid crystals in living matter. *Soft Matter*, **13**, 4176–4209.

60. Leforestier,A., Bertin,A., Dubochet,J., Richter,K., Sartori Blanc,N. and Livolant,F. (2008) Expression of chirality in columnar hexagonal phases or DNA and nucleosomes. *Comptes Rendus Chim.*, **11**, 229–244.

61. Ho,P.S. (2017) Structure of the Holliday junction: applications beyond recombination. *Biochem. Soc. Trans.*, **45**, 1149–1158.

62. Ho,P.S. and Eichman,B.F. (2001) The crystal structures of DNA Holliday junctions. *Curr. Opin. Struct. Biol.*, **11**, 302–308.

63. Mishra,A. and Hawkins,R.D. (2017) Three-dimensional genome architecture and emerging technologies: Looping in disease. *Genome Med.*, **9**, 1–14.

64. Smith,C.A. and Vinograd,J. (1972) Small polydisperse circular DNA of HeLa cells. *J. Mol. Biol.*, **69**, 163–178.

65. Shibata,Y., Kumar,P., Layer,R., Willcox,S., Gagan,J.R., Griffith,J.D. and Dutta,A. (2012) Extrachromosomal microDNAs and chromosomal microdeletions in normal tissues. *Science*, **336**, 82–86.

66. Kumar,P., Dillon,L., Shibata,Y., Jazaeri,A.A., Jones,D.R. and Dutta,A. (2017) Normal and cancerous tissues release extrachromosomal circular DNA (eccDNA) into the circulation. *Mol Cancer Res.*, **15**, 1197–1205.

67. Paulsen,T., Shibata,Y., Kumar,P., Dillon,L. and Dutta,A. (2019) Small extrachromosomal circular DNAs, microDNA, produce short regulatory RNAs that suppress gene expression independent of canonical promoters. *Nucleic Acids Res.*, **47**, 4586–4596.

68. Gaubatz,J.W. (1990) Extrachromosomal circular DNAs and genomic sequence plasticity in eukaryotic cells. *Mutat. Res. DNAging*, **237**, 271–292.

69. Gaubatz,J.W. and Cutler,R.G. (1990) Mouse satellite DNA is transcribed in senescent cardiac muscle. *J. Biol. Chem.*, **265**, 17753–17758.

70. Gaubatz,J.W. and Flores,S.C. (1990) Tissue-specific and age-related variations in repetitive sequences of mouse extrachromosomal circular DNAs. *Mutat. Res. DNAging*, **237**, 29–36.

71. Turner,K.M., Deshpande,V., Beyter,D., Koga,T., Rusert,J., Lee,C., Li,B., Arden,K., Ren,B., Nathanson,D.A. *et al.* (2017) Extrachromosomal oncogene amplification drives tumour evolution and genetic heterogeneity. *Nature*, **543**, 122–125.

72. Morton,A.R., Dogan-Artun,N., Faber,Z.J., MacLeod,G., Bartels,C.F., Piazza,M.S., Allan,K.C., Mack,S.C., Wang,X., Gimple,R.C. *et al.* (2019) Functional enhancers shape extrachromosomal oncogene amplifications. *Cell*, **179**, 1330–1341.

73. Shoura,M.J., Gabdank,I., Hansen,L., Merker,J., Gotlib,J., Levene,S.D. and Fire,A.Z. (2017) Intricate and cell type-specific populations of endogenous circular DNA (eccDNA) in Caenorhabditis elegans and homo sapiens. *G3 Genes|Genomes|Genetics*, **7**, 3295–3303.

74. Dekker,J., Belmont,A.S., Guttman,M., Leshyk,V.O., Lis,J.T., Lomvardas,S., Mirny,L.A., O'Shea,C.C., Park,P.J., Ren,B. *et al.* (2017) The 4D nucleome project. *Nature*, **549**, 219–226.